Pre-wave zone studies of Coherent Transition and Diffraction Radiation

V. Shpakov [a,*], M. Bellaveglia [a], M. Castellano [a], E. Chiadroni [a], A. Cianchi [a,b], S. Dabagov [a,e,f], D. Di Giovenale [a], M. Ferrario [a], F. Giorgianni [c], S. Lupi [c], A. Mostacci [d], M. Petrarca [d], G. Di Pirro [a], R. Pompili [a], F. Villa [a]

[a] INFN Laboratori Nazionali di Frascati, Frascati, Italy
[b] University of Rome "Tor Vergata" and INFN-RM2, Rome, Italy
[c] Department of Physics, Sapienza University of Rome, Rome, Italy
[d] SBAI Department, Sapienza University of Rome, Rome, Italy
[e] RAS P.N. Lebedev Physical Institute, Moscow, Russia
[f] NRNU MEPhI, Moscow, Russia

ABSTRACT

Advanced accelerator technology, based on plasma structures, requires high brightness electron beams, which can be used also to drive advanced radiation sources. Indeed, electron beams to be injected into the plasma and accelerated in the plasma channel are characterized by small transverse size and ultra-short time duration, allowing the production of coherent radiation in the THz range. In the present work we report both theoretical and experimental studies on the spatial/angular distribution of Coherent Transition and Diffraction Radiation in the pre-wave zone.

© 2015 Elsevier B.V. All rights reserved.

1. Introduction

Transition and Diffraction radiation (TR and DR, respectively), though deeply investigated, still excite great interest from their widely use in electron beam diagnostics, due to a strong dependence of intensity and angular distribution on beam size, angular divergence and energy. In addition, TR and DR, generated by ultra-short (sub ps) electron beams, is increasingly used as source of coherent THz radiation for a wide variety of applications spanning from science to biology, from medicine to industry [1]. Therefore a great interest is growing in the optimization of compact sources of intense THz radiation as those driven by plasma-based accelerators. In the present work we investigate numerically and experimentally the spatial/angular distribution of both coherent transition (CTR) and diffraction (CDR) radiation in pre-wave zone as produced at the SPARC_LAB test facility [2] by high brightness electron beams as needed for particle driven plasma acceleration. First measurement of CDR spatial distribution at THz frequencies are also reported.

After a brief history about TR and DR observation, in Section 2 we introduce the theoretical background, needed for introducing and discussing the model we developed in order to validate the measurement. In Section 3 we describe the experimental geometry and apparatus used to acquire the CTR/CDR spatial distribution, and we report the electron beam longitudinal phase space optimized for the production of THz radiation. Section 4 is dedicated to the comparison of measurement data with numerical model at different THz frequencies. Finally, the results are discussed in Section 5.

2. Theory and simulations

Transition radiation is emitted when a charge particle crosses the boundary between two media with different dielectric constants. The theory of TR was discussed in several works [3,4]. The first analytical expression for TR angular distribution was obtained in [3] and today it is widely known as Ginzburg–Frank formula. Diffraction radiation was first observed on periodical structure and today this special case of the DR is called Smith–Purcell radiation [5]. Later the DR was studied in [6,7], where the "pseudo photon" method[1] was used in order to obtain the analytical expression for DR angular distribution. In both cases the radiation was considered under several conditions, such as infinite perfectly

---

[1] Weizsacker–Williams method of virtual quanta [8], where the electron field is replaced with equivalent electromagnetic wave.

* Corresponding author.

conducting target and wave zone approximation, which impose some restriction on the field of application. Later further studies were conducted in order to generalize the obtained results beyond the ideal conditions, therefore finite screen size and observation in pre-wave zone [4,9–11]. Here and further we use terms wave and pre-wave zones as they were used by Verzilov in [9].

The wave zone approximation for TR and DR can be applied if several conditions are satisfied. The detector should be placed beyond the pre-wave zone of radiation with respect to the source. For TR and DR the size of the pre-wave zone can be estimated as minimum out of $\lambda\gamma^2$ or target size, here λ is the wavelength of radiation and γ is the Lorentz factor of the bunch. In approximation of the infinite screen, for THz radiation wavelength and for electron beam with energy of the order of 100 MeV the wave zone condition is satisfied at several meters from the source. Thus, in most of the cases, we can work either in a pre-wave zone or we should use a suitable optical system. In order to use the infinite screen approximation the conditions should be imposed on the target size. The TR and DR can be considered as an interaction between electron field and the target material. At high energy, due to the relativistic effects, the electron field becomes a flat disc in a plane perpendicular to the electron velocity vector, whose "effective" size can be estimated as $\sim \lambda\gamma$ [4,11,12]. For the wave zone approximation [3,6] the size of the target was considered as infinite with respect to the electron field, and in order to satisfy this condition the size of the target should be larger than the effective size of the electron field. For optical wavelengths this condition is normally achieved even at GeV energies, while for THz wavelengths the effective size of the field can be either comparable with the size of the target or exceed it, even at low electron beam energies, i.e. few hundreds MeV. Thus for THz radiation the size of the pre-wave zone at some point may be given by the size of the target. In this work pre-wave zone effects as well as effects caused by finite screen size with respect to the effective size of the field have been studied theoretically and experimentally, and the measured CTR/CDR spatial distribution compared with the numerical model.

In our work the pseudo photons approach is used. The field of the particle is considered as consisting of pseudo photons, which become real during the interaction with the target material [12]. For ultrarelativistic electrons ($\gamma \gg 1$) the transverse components of the electric field of the single particle can be written as:

$$E^e_{x,y} = \frac{e\omega}{\pi\gamma v^2} \frac{x,y}{\rho} K_1\left(\frac{\omega\rho}{v\gamma}\right), \tag{1}$$

where e is the electron charge, ω is the radiation angular frequency, v is the particle velocity, $\rho = \sqrt{x^2 + y^2}$, with x and y the coordinates in the plane perpendicular to the beam trajectory, $E^e_{x,y}$ is the component of the electric field along X and Y (Fig. 1), k is the wave vector, and K_1 the modified Bessel function of the second kind. In the following simulations the longitudinal component of the electron field was neglected, being γ times smaller. As particular case we will consider DR emission. According to the pseudo photons method we replace the electron field with electromagnetic wave. Thus the outgoing radiation can be considered as scattering on the target and calculated by the Huygens–Fresnel principle:

$$E^i_{x,y}(x',y',\omega) = -\frac{ik}{2\pi}\int_{-b/2}^{b/2}\int_{-a/2}^{-d/2} E^e_{x,y}(x,y)\frac{e^{ikR}}{R}dxdy + \frac{ik}{2\pi}\int_{-b/2}^{b/2}$$
$$\times \int_{d/2}^{a/2} E^e_{x,y}(x,y)\frac{e^{ikR}}{R}dxdy, \tag{2}$$

where x', y' are the coordinates of the observation point, $R = \sqrt{Z^2 + (x'-x)^2 + (y'-y)^2}$, and Z is the distance from the target to the observation plane. Here a and b are the sizes of the rectangular target and d is the size of the slit in it. The two integrals
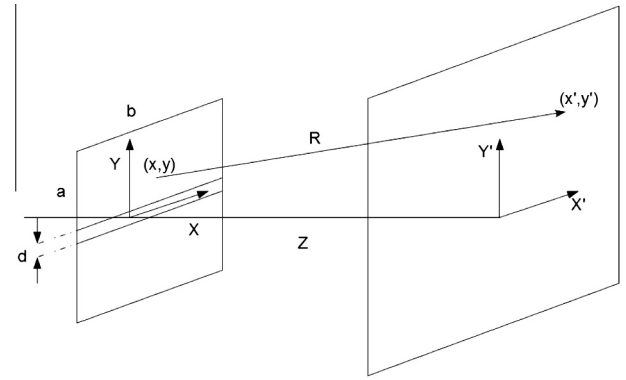

Fig. 1. Diffraction radiation geometry.

in Eq. (2) represent the DR field from the two semi-planes. In case of effective field size smaller than the target size, the finite limits in the integrals would tend to infinite.

So far a single electron has been considered. In practice, we have to deal with a beam of N electrons (typically $N \approx 10^9$). The full intensity of radiation, basically any kind of radiation, emitted by a beam of N electrons can be presented in the following form:

$$I(\omega) = I_e(\omega)[N + N(N-1)F(\omega)], \tag{3}$$

where $I_e(\omega)$ is the radiation emitted by a single electron, and $F(\omega)$ is the beam form factor. The beam form factor, in general, is the Fourier transformation of the normalized 3D distributions, and characterizes the level of coherence with respect to the radiation: the completely incoherent beam has form factor equal to 0, while 1 corresponds to completely coherent beam. In the cases reported in the paper the full form factor is replaced with its longitudinal component F_l, because the contribution of the transverse one is negligible [13]:

$$F_l(\omega) = \left|\int S_l(z)e^{-\frac{i\omega z}{c}}dz\right|^2, \tag{4}$$

where $S_l(z)$ is the normalized beam longitudinal distribution, and c is the speed of light. Therefore coherent radiation is observed at wavelengths larger than the beam longitudinal size. In the THz region coherent radiation can be produced by beams, whose bunch duration is of the order of 100 fs and less. Here we assume a beam with Gaussian longitudinal distribution. For simulations the DR target made of 2 half planes (3×3 cm each) separated by a 3 mm gap was used, while the effective size of the field for used parameters (i.e. $\gamma = 200$ and $\lambda = 600$ μm, corresponding to 0.5 THz radiation frequency) is $\lambda\gamma \approx 12$ cm. In our work frequencies up to 5 THz and lower were considered. At low frequencies, such as 0.5 THz, the beam form factor is close to 1, which allows to consider a completely coherent beam for simulations. For the higher frequencies the beam form factor is less than 1. The spectral-angular distribution in the pre-wave zone has been calculated by means of the following expression:

$$\frac{d^2U}{d\omega d\Omega} = cR^2\left[\left(\sum_{i=1}^{N}E^i_x\right)^2 + \left(\sum_{i=1}^{N}E^i_y\right)^2\right], \tag{5}$$

where N is the total number of electrons in the bunch, $E^i_{x,y}$ is the electric field component of radiation emitted by the single particle (Eq. (2)) and Ω is the solid angle. The simulation results for the vertical component are presented in Fig. 2a and b and show the dependence of CDR angular distribution on the distance Z between the source and the detector. The CDR angular distribution in pre-wave

zone presents a significant angular broadening if compared to the distribution calculated in wave zone approximation.

The difference disappears very quickly with increasing the distance and the distribution resembles to the one for the wave zone. The simulation results for CDR angular distribution at different distances from the source are shown Fig. 2a. Both a significant angular broadening of the distribution and a decreasing of intensity for short distances between the source and the detector plane are clearly observed.

The position of the maxima of the CDR angular distribution is reported as a function of the distance between source and detector plane in Fig. 2b. The behavior of the CDR distribution is quite similar to that of CTR distribution, which was studied in [9,14]. At distances larger than 1 m the maxima positions practically become equal to those of the wave zone approximation and practically do not change with further increasing the distance. However, this result is not in agreement with position of maxima equal to $\sim 1/\gamma$ and wave zone condition $\sim \lambda\gamma^2$, as expected for angular distribution calculated in the wave zone approximation. Such differences are caused by the finite size of the screen with respect to the spatial extension of the electron field. The effect of the screen finite size on the TR angular distribution in the wave zone was first highlighted in [15]. The dependence of the angular distribution maxima position on the ratio between target size and effective field size is depicted in Fig. 3a. The position of the maxima for 20 cm screen size ($\gg \gamma\lambda$) is $\sim \pm 4.5$ mrad, corresponding to the expected angle $1/\gamma$. The wave zone distribution maxima position for the 3 cm screen ($< \gamma\lambda$) is $\sim \pm 16.5$ mrad which is significantly larger than the expected $1/\gamma$. Moreover, when the ratio between target size and field size is less than 1, the angular distribution resembles to the one calculated in the wave zone at $Z \ll$ than the $\lambda\gamma^2$. For the 3 cm screen wave zone angular distribution was obtained at distance larger than 2 m instead of $\lambda\gamma^2 \approx 24$ m. The results of simulations described above are mainly connected to the CDR, however, the used model can be also applied to simulate CTR. to do so is enough to put size of the gap to 0, since the TR target tends to a DR one with null slit aperture, and CDR angular distribution will turn into CTR one.

Experimentally, a bandpass filter, inserted in front of the detector, was used in order to measure CTR/CDR at the desired frequency (Fig. 3b). Since the spatial/angular distribution can be affected by the finite filter bandwidth, in our simulation the emission is considered as Gaussian distributed around the filter central frequency. The total intensity for the full spectrum was calculated as a sum of radiation at all frequencies. Thus the total intensity can be written in the form:

$$\frac{dU_{tot}}{d\Omega} = \int_{-\infty}^{+\infty} e^{\frac{-(\omega_0 - \omega)^2}{2\sigma^2}} \left(\frac{d^2 U}{d\omega d\Omega} \right) d\omega, \tag{6}$$

where σ is FWHM of the bandwidth of the filter, ω_0 is the filter central frequency and radiation for selected frequency is expressed by Eq. (5). The coefficient at the spectral-angular distribution inside the integral shows the transmittance of the filter for a given frequency. The most significant difference, beside the intensity, between CDR distribution for the full spectrum and selected frequency is a lack of secondary maxima (Fig. 3b). The tails of the full spectrum CDR distribution are smooth and slightly wider than one for the single frequency.

3. Experimental setup

The experiment was carried out at the SPARC_LAB test facility at Laboratori Nazionali di Frascati. The SPARC linac consists of a photocatode RF-gun, 3 S-band traveling wave (TW) accelerating sections, able to provide electron beams with energy up to

170 MeV, 100s pC charge, at 10 Hz repetition rate. For the measurements presented here, the first accelerating section has been used as RF compressor, in the so-called Velocity Bunching (VB) regime, based on a time-velocity correlation in the electron bunch which causes electrons in the bunch tail to be faster than electrons in the bunch head. If the beam is slightly slower than the phase velocity of the RF wave, when injected at the zero crossing field phase, it slips back to phases where the field is accelerating and, simultaneously, it is chirped and compressed [16]. Under this operational regime the 200 pC beam was longitudinally compressed down to 100 fs (rms), with a final energy 113.8 MeV. The measured longitudinal phase space of the bunch is shown in Fig. 4a.

Coherent radiation, both transition and diffraction, is generated at SPARC_Lab, by such ultra-short electron beams for longitudinal diagnostics and THz experiments [17,18]. The experimental geometry is shown in Fig. 4b: the target is aluminum coated silicon screen tilted to $\pi/4$ with respect to the beam trajectory for the radiation extraction. TR screen is the square plate with size of 3×3 cm. DR target consist of two rectangular plates 3×2 cm size with 3 mm gap between them. Both targets were placed into the vacuum chamber, large enough to avoid any boundary effects. Measurements were performed for both CTR and CDR, at frequencies 0.5, 3 THz and with no filters. The emitted radiation goes through the z-cut quartz window, directly to the pyrodetector. In order to select one of the frequency the filters were mounted right in front of the pyrodetector (Gentec-EO THZ2I-BL-BNC). The transmittance bandwidth is Gaussian distribution with dispersion $\sim 20\%$ of the central frequency. The detector was working in linear regime. The experiment was carried out in air, which led to significant absorption of radiation, however, for our measurement intensity of radiation was not important – only the radiation distribution. In order to obtain the distribution of the radiation the detector was mounted on the XY-axis stage in order to map (scan) the area of interest. Size of the scanning area was up to 46×46 mm with scanning step 1 or 2 mm.

4. Results

The CTR spatial distribution at 0.5 THz was measured at two distances from the source, i.e. 9 cm (Fig. 5) and 55 cm (Fig. 5b). Experimental data (red dots[2]) are compared to simulation results (blue line), showing a good agreement in the position of maxima.

The CDR angular distribution was measured in the pre-wave zone as well, as shown in Fig. 6a. The position of the maxima of the simulated distribution is in good agreement with the experimental results. In Fig. 6b the spatial distribution for the CTR at 3 THz frequency is shown. Results of those measurements also were compared with calculations based on Eqs. (5) and (6). For the 100 fs beam, the form factor at 3 THz is significantly lower than 1, but the theoretical calculations still are in a good agreement with the experimental data. However, the estimation of the form factor is valid only for the Gaussian beam distribution, while the experimental beam shape was more triangular (Fig. 4a). The slopes of the experimental beam distribution is steeper than for the Gaussian one, which makes the actual form factor of the beam much higher. The general instability of the intensity of the experimental data for both 3 THz and 0.5 THz radiation can be caused by prolonged time of acquisition, for which any beam instability, e.g. charge fluctuation, energy jitter, RF compression phase instability might affect the results.

In addition, there are two main differences between the experimental results and theoretical indication. The intensity at

---

[2] For interpretation of color in Fig. 5, the reader is referred to the web version of this article.
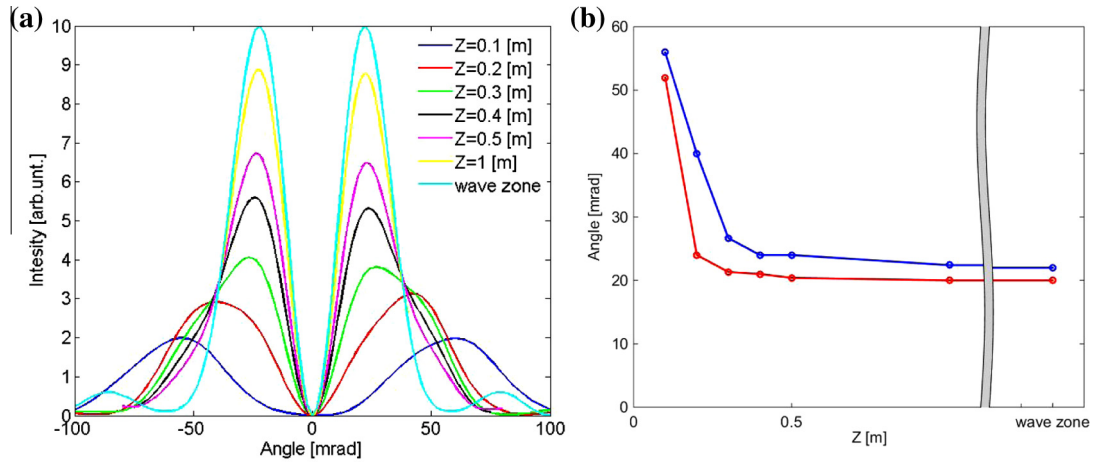
Fig. 2. (a) CDR angular distributions for different distances for radiation frequency 0.5 THz and beam energy 100 MeV. Slit aperture is 3 mm and Z is the distance between the source and the detector. (b) Dependence of maxima position on the distance Z between the source and the detector calculated for a frequency of 0.5 THz, beam energy 100 MeV, and size of the target 3×3 cm, with 3 mm aperture in case of CDR.
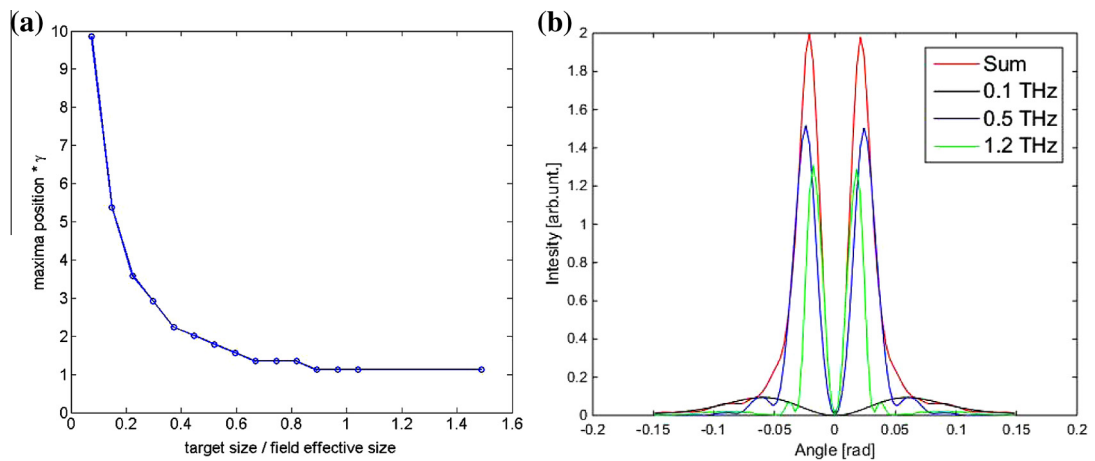

Fig. 3. (a) Angular distribution maxima position of the wave zone CDR angular distribution as function of the ratio between target size and effective size of the field. The maxima position is normalized to $1/\gamma$. (b) The angular distribution of the CDR in the frequency range 0.1–1.2 THz and full spectrum transmitted through the 0.5 THz filter (red line). The intensity for given frequency is multiplied by factor 5 due to the low intensity. (For interpretation of the references to color in this figure legend, the reader is referred to the web version of this article.)
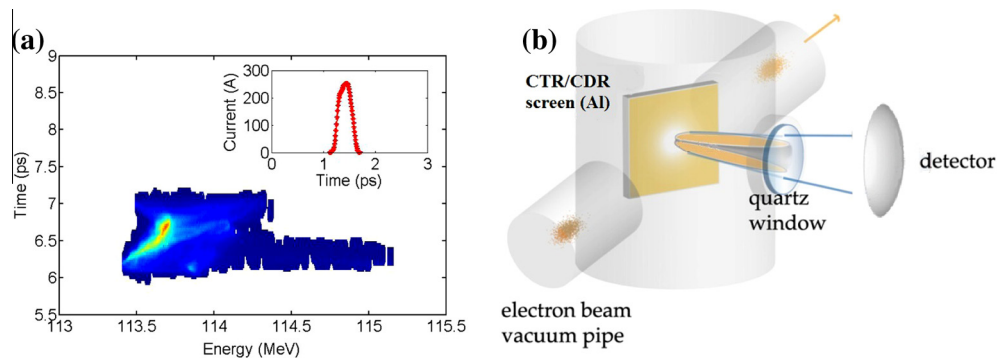

Fig. 4. (a) Measured longitudinal Phase Space of the bunch (inset – longitudinal beam profile) and (b) Sketch for the TR setup at SPARC facility.

the center of the distribution is expected to be zero, or at the level of the noise. The experimental results for both CTR (Fig. 4a) and CDR does not show such behavior. In addition the width of the maxima is slightly broader than expected. Both disagreements could be caused by the low spatial resolution of the detector. The step of the scanning during the experiment was 1 or 2 mm, while the size of the distribution for CDR as well as

for CTR at 9 cm from the target was around 2–3 cm for radiation with 0.5 THz frequency, and even less for 3 THz radiation. The CTR distribution at the distance 55 cm from the target has a much larger size, which makes the relative resolution better, as a consequence the experimentally measured minimum in the center is much closer to the zero, as it is predicted by the theory (Fig. 5b).

(a) Distance to the detector 9 cm, scanning step 1 mm. (b) Distance to the detector 55 cm, scanning step 2 mm.
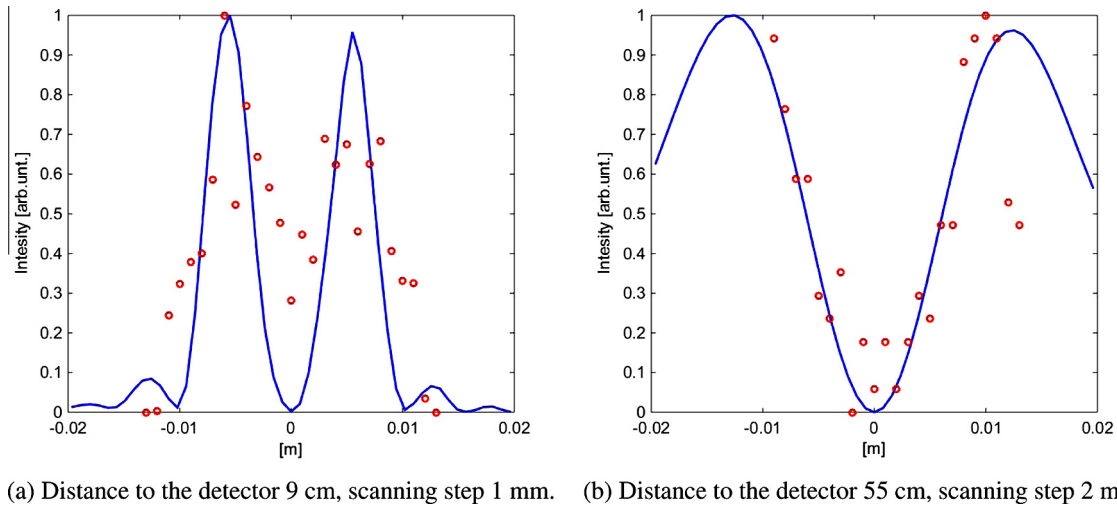
Fig. 5. The CTR spatial distribution at two different distances from the target. Blue curves are results of simulations and red dots are experimental results. The frequency of the radiation is 0.5 THz, beam energy 113.8 MeV, beam charge 200 pC. (For interpretation of the references to color in this figure legend, the reader is referred to the web version of this article.)
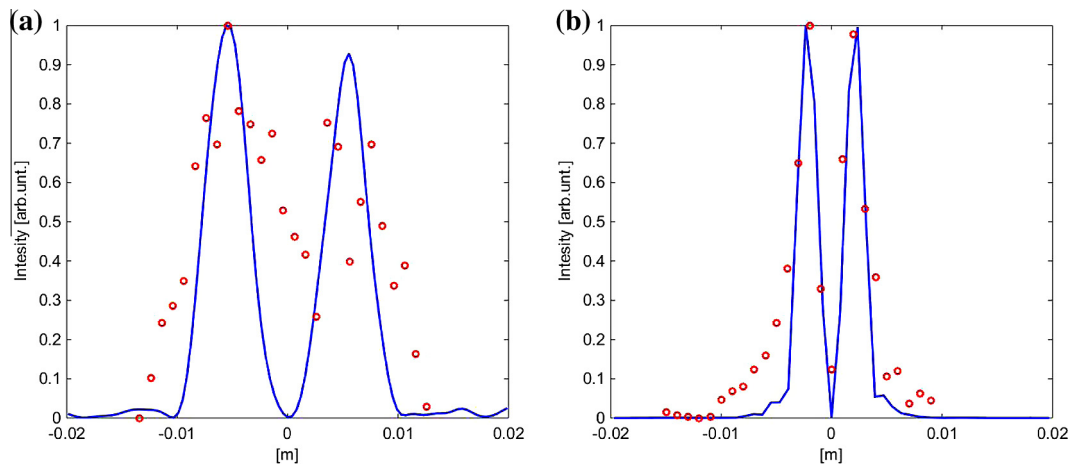
Fig. 6. (a) The 0.5 THz CDR spatial distribution at 9 cm distance. Blue curve is results of simulations and red dots are experimental results. (b) The spatial distribution of the CTR at 3 THz at 9 cm from the source. (For interpretation of the references to color in this figure legend, the reader is referred to the web version of this article.)

5. Conclusion

The angular/spatial distribution of the CDR and CTR in THz spectrum region has been studied. The simulation results have shown significant dependence of both wave zone and pre-wave zone distribution on size of the screen. Using a target smaller than the effective size of the electron field leads to significant broadening of the distribution in wave zone. More over, since the transverse size of the source is the reason why radiation needs to propagate certain distance before acquiring all wave zone properties, the limit of the wave zone also may vary. In case of THz radiation, when the electron effective field can be significantly larger than size of the target, the size of the pre-wave zone may change as well. In considered cases, the radiation angular distribution resembles to the one in wave zone at 2–3 m from the source instead of expected $\lambda\gamma^2 \approx 20$–$25$ m.

The results of the theoretical calculations are in good agreement with the experimental results. The existing deviations of the experimental results from theoretical calculations can be explained by the resolution of the experimental apparatus. However, the maxima position of the theoretical CTR and CDR distribution always are in a good agreement with experimental distribution.

Acknowledgements

References

[1] M.S. Sherwin, C.A. Schmuttenmaer, P.H. Bucksbaum, Opportunities in THz science, Report of a DOE-NSF-NIH Workshop, 2004.
[2] M. Ferrario et al., Nucl. Instr. Meth. Phys. Res. B 309 (2013) 183.
[3] I. Frank, J. Ginsburg, J. Phys. USSR 9 (1945) 353.
[4] A.P. Potylitsyn, Nucl. Instr. Meth. Phys. Res. B 145 (1998) 169–179.
[5] S.J. Smith, E.M. Purcell, Phys. Rev. 92 (1953) 1069.
[6] M.L. Ter-Mikaclian, High Energy Electromegnetic Processes in Condensed Media, Wiley-Interscience, New York, 1972.
[7] B.M. Bolotovskii, E.A. Galstyan, Phys. Usp. 43 (2000) 755.
[8] C.F. Weizscker, Z. Phys. 88 (1934) 612.
[9] V.A. Verzilov, Phys. Lett. A 273 (2000) 135–140.

[10] S.N. Dobrovolsky, N.F. Shul'ga, Nucl. Instr. Meth. Phys. Res. B 201 (2003) 123132.
[11] M. Castellano et al., Phys. Rev. E 67 (2003) 015501(R).
[12] J.D. Jackson, Classical Electrodynamics, John Wiley & Sons, New York, 1998.
[13] O. Grimm, P. Schmuser, TESLA FEL Reports 2006-03, 2006.
[14] Changmook Yim et al., Phys. Rev. Spec. Topics Accelerat. Beams 15 (2012) 030706.
[15] S. Casalbuoni, B. Schmidt, P. Schmuser, V. Arsov, S. Wesch, Phys. Rev. Spec. Topics Accelerat. Beams 12 (2009) 030705.
[16] L. Serafini, M. Ferrario, AIP Conf. Proc. 581 (2001) 87.
[17] E. Chiadroni et al., Rev. Sci. Instr. 84 (2013) 022703.
[18] E. Chiadroni et al., Appl. Phys. Lett. 102 (2013) 094101, http://dx.doi.org/10.1063/1.4794014.